Nuclear Mathematical and Computational Sciences: A Century in Review, A Century Anew
Gatlinburg, Tennessee, April 6-11, 2003, on CD-ROM, American Nuclear Society, LaGrange Park, IL (2003)

APPLICATION OF MCNP CALCULATIONS TO CALIBRATION OF ANTHROPOMORPHIC PHANTOMS USED FOR ASSESSMENT OF ACTINIDES IN LUNGS

N. Borisov
Institut de Radioprotection et de Sûreté Nucléaire
B.P. 17, F-92262, Fontenay-aux-Roses Cedex, France
nikolai.borissov@irsn.fr

State Research Center — Institute of Biophysics
46, Zhivopisnaya street, 123182, Moscow, Russia
nikolai_borissov@hotmail.com

D. Franck, L. de Carlan and N. Pierrat
Institut de Radioprotection et de Sûreté Nucléaire
B.P. 17, F-92262, Fontenay-aux-Roses Cedex, France
didier.franck@irsn.fr, loic.decarlan@irsn.fr

V. Yatsenko
State Research Center — Institute of Biophysics
46, Zhivopisnaya street, 123182, Moscow, Russia
yatsenko@srcibph.ru

ABSTRACT

The paper reports on a new utility for development of computational phantoms for Monte Carlo calculations and data analysis for *in vivo* measurements of radionuclides deposited in tissues. The individual dimensions of each worker can be acquired for a rather precise geometric representation of his (her) anatomy, which is particularly important for low energy gamma ray emitting sources such as thorium, uranium, plutonium and other actinides. The software discussed here enables automatic creation of an MCNP^{TM} input data file based on CT or MRI images. The utility was firstly tested for low and medium energy actinide emitters on anthropomorphic phantoms, the mannequins generally used for *in vivo* counting, in order to compare the results of simulation and measurement. From these results, the demonstration of the utility's abilities for the study of geometry uncertainties, such as different anthropomorphic phantoms or different source geometries, on *in vivo* calibration was investigated. Calculations and comparison with the experimental data are presented and discussed in this paper.

Key Words: lung counting; actinides; Monte Carlo; physical phantom; voxel phantom

1. INTRODUCTION

Being the method for direct measurement of the patient, *in vivo* lung measurement is the preferred technique for estimating contamination after the inhalation of radiotoxic substances. Actinides (particularly ^{239}Pu) emit low energy x-rays and gamma rays. Although detection has been improved by the introduction of the large area germanium detector, equipment performance results in measurement uncertainties that are still far too high [1]. Although great efforts have been made to improve the physical phantoms used for

calibrating *in vivo* measurement systems, they actually represent only an approximate geometry and generally only provide for uniform distribution of radionuclides in contaminated tissue.

In addition, the high attenuation of photons of energies between 10 and 100 keV in human tissue constitutes a major obstacle to the detection of the radionuclides responsible for contamination. Therefore, knowledge of the thickness of the chest wall and of its composition (which caould be taken, e.g., from the ICRU publication 44 [9]) is crucial to the correct estimation of the calibration factors for a given individual. In general, thickness is estimated by ultrasonic methods or by bioparametric measurements essentially consisting of weight and height [2, 3]. However, such procedures lack the necessary accuracy to properly cover biological differences such as the proportion of fat, and make no allowance for other differences, such as organ size and chest wall thickness variation along the thorax. It is, therefore, important to develop new calibration techniques that are more adaptable to such variations, and earlier work has shown the possibility of using the Monte Carlo method [4, 5].

The purpose of the work described here is to show the potential for the construction of computational phantoms using anatomical and physiological data relating to individuals to be measured, with the longer-term goal of flexible use in a large number of different applications such as measurement as wound, thyroid and lung measurement. This involves an original calibration method that has been developed, combining the creation of numerical phantoms in the form of voxels obtained from tomography images (CT) or magnetic resonance images (MRI) with Monte Carlo calculations [6]. This calibration method involves the use of a graphical user interface (Anthropo) specially developed with the PV-Wave® [7] software. The Monte Carlo code used is MCNP4c^{TM} [8], which simulates the transport of photons with energies corresponding to the range of interest (i.e. 10 to 1400 keV) through tissue.

2. DESCRIPTION OF *ANTHROPO* INTERFACE

The *Anthropo* interface enables automatic creation of MCNP4c^{TM} input file on the base of magnetic resonance or CT scanner images as well as source and detector description, specified by the physicist in charge of measurement. It is specially designed for the data required for MCNP4c^{TM} to simulate spectra.

The data processed by the *Anthropo* interface consists of three parts: (i) magnetic resonance or scanned images of a phantom or a person, (ii) source description, i.e. the type of source (point or diffuse), the number of gamma-quanta emitted, their energy, probability, calculated automatically from the activity of the source and time of measurement, and finally, (iii) the geometry of the detector and its positioning relative to the numerical phantom.

In addition to the basic arrangement, there are modules for saving information, and for image processing and display. The images obtained from the scanning device are first processed with special software called DOSIGRAY® (a treatment planning system used in radiotherapy, provided by Gustave Roussy Cancer Research Institute in Villejuif), which allows segmentation of organs and tissues by surrounding contours, on the basis of different shades of grey obtained when creating images by tomography or magnetic resonance. The segmentation with DOSIGRAY® is followed by importation of the contours into the *Anthropo* program. The segmentation can also be done directly in *Anthropo* but it is generally less convenient. For these segmented images, *Anthropo* performs association of different organs with the their proper che;ical compositiontissue densities specified by ICRU [9].

The MCNP4c^{TM} input file is then automatically written by the *Anthropo* interface which represents one of its major features. The procedure of unput file creation was discussed and described in [6]. It implies coupling neighbor voxels with the same chemical composition and density into larger rectangular boxes. The tally to be calculated is F8 with GEB option. The size of energy bin and energy calibration can be adjusted to the individual measurement before creation of MCNP^{TM} input file. The input file consists of the above data plus data relating to the geometry of the detector and the materials it is made of, the nature of the sources and, finally, the quantities required from the calculations (referred to as the "tally" in MCNP), i.e. in our case, the spectrum of the energy deposited in the counter. This stage is completely automatic. To check that the MCNP4c^{TM} input file is properly configured, the overall geometry (phantom + detector) is displayed using the Sabrina® code [10].

Additional functions have been also added into the interface, namely a tool for output data processing to perform subsequent spectrometric analysis: plotting the spectrum, performing integral calculation in Region of Interest and making a direct comparison with the experimental spectrum. This module is not very advanced but is very convenient to treat data and compare it with measurements.

The flexibility of *Anthropo* regarding to the input data, particularly the type of phantom and the sources, should make it possible to use it both for diagnoses and for *in vivo* counting in cases of actual contamination or studies of non-uniform contamination, as well as for optimization of detector positioning.

3. VALIDATION AND APPLICATION OF *ANTHROPO* INTERFACE

This paper describes and discusses the demonstration of *Anthropo* abilities for *in vivo* calibration during three series of experiments and calculations. First, the agreement between real measurement and mathematical simulation results was checked. Then, the dependence of simulated results for variation of phantom geometries was demonstrated. Finally, the calibration for heterogeneous (surface and point) contamination in lungs was analyzed.

3.1. Ability of *Anthropo* to perform low-energy lung measurements

The procedure was first validated for specific case of low-energy lung measurements on Livermore phantoms [11], the mannequins generally used in *in vivo* counting, in order to compare the results of simulation and measurement. The measurement has been performed using uniformly contaminated lungs containing 70 kBq of ^{241}Am and 80 Bq of 93% enriched ^{235}U with high purity low energy germanium (LEGe) gamma-spectrometer "Canberra Semiconductors NV", placed in front of the middle of the right lung. The diameter of the detector is 50.5 mm, width — 20 mm, window thickness — 0.5 mm; no anti-compton shield used. The calculation has been made under the same conditions using scanner images of the phantom performed at *Hôpital d'Instruction des Armées Percy* in Clamart near Paris. The geometry has been reconstructed, written as MCNP^{TM} input file by *Anthropo* and then visualized with Sabrina® to check the whole procedure. All the cracks in the phantom were taken into account. Number of voxels in the CT image was $256\times256\times40$.

The experimental and calculation full absorption peak (59.54 keV ^{241}Am for 185.72 keV for ^{235}U) intensities, normalized per 1 second and 1 kBq source, are presented in Table I. The difference between absolute value of full absorption peak intensity for measurement and MCNP^{TM} calculations is about 12% for ^{241}Am and 14% for ^{235}U. To avoid considerable attenuation, no plate was used with the Livermore phantom in experimental test.

Table I. Principal full absorption peak intensities for ^{241}Am and ^{235}U in lung of Livermore phantom, signals$\times$s$^{-1}\times$kBq^{-1}

Energy	Experiment	Calculation	Difference
^{241}Am, 59.54 keV	0.849	0.749	-12%
^{235}U, 185.72 keV	1.062	0.909	-14%

Calculated and measured spectra obtained for 70 kBq of ^{241}Am and 600 s of measurement are presented in Fig. 1. The spectrum (from output file tool processing of *Anthropo*) is expressed in terms of counts per channel. The calculation is performed exactly under the same conditions as the measurement: geometry, activity, time of measurement and channel width to compare directly the absolute experimental and calculated spectra. No special efficiency correction or spectrum normalization (except Gaussian broadening) was applied. There is good agreement between the experimental data and simulation both in the full absorption peak of the most intensive ^{241}Am line (59.54 keV) and in the Compton scattering area. The standard deviation in the spectrometric channel with maximal intensity is about 8% for 1,000,000 histories, which take 5 h 15 min of calculation for DEC Alpha® Compaq® professional workstation (frequency 500 MHz, memory 1 Gb).

The comparison of calculation (white line) and experimental (dark line) spectra for lung contamination with 80 Bq of ^{235}U and 600 s of measurement is presented in Fig. 2 (from output file processing tool of *Anthropo*, number of voxels: $256\times256\times40$). In order to fit better to a real spectrum, natural background measured independently without source, was added to calculation spectrum. There is good agreement between experiment and pseudo-calculation in full absorption peaks for major energies of rays emitted by ^{235}U.

3.2. Application of *Anthropo* for phantom intercalibration

The potential of this approach to study uncertainties influencing lung counting results was shown by comparison of calculated efficiency for both “low” and “high” energies with different phantoms scanned and processed with *Anthropo*. For this study, no experimental measurements were done. The digital phantoms were derived from CT images. To provide the uniformity of calculations, and to study the influence of pure geometric parameters on phantom calibration, for all of the phantoms distinguish muscle and fat tissues were not distinguished, and all soft tissues were assigned as muscle.

The characteristics of the scanned phantoms are shown in Table II, description of three principal distances — in Fig. 3. Weight and height are taken from ICRU Report 48 [11], other parameters obtained with DOSIGRAY®. The segmented images of the phantoms used (as well as photos of them) are shown in Fig. 4 corresponding to: Livermore National Laboratory plastic chest phantom, JAERI Japanese plastic phantom, RANDO whole body phantom, Winfrith Technology Center (UK) hollow plastic torso phantom, filled with tissue-equivalent powder, as well as the image of a real male patient weighing 74 kg, respectively. All the cracks of the phantoms were taken into account. To fit the anatomy of the patient, the Livermore phantom was used with the plate #3 (series B), and the JAERI phantom — with the 3.6 cm thick

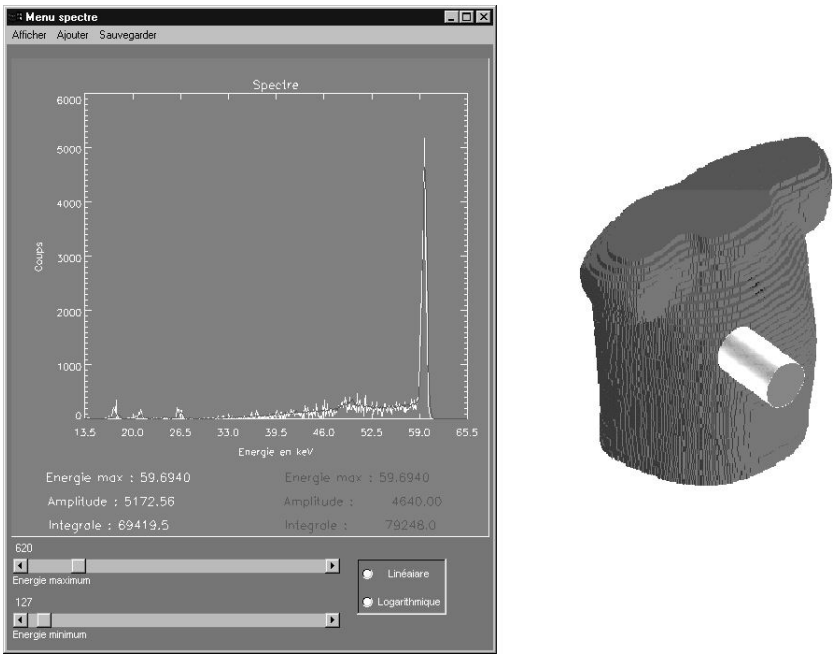

Figure 1. On the left: comparison of experimental (dark line) and MCNP$^{\mathrm{TM}}$ (white line) pulse-height-spectrum for 70 kBq ^{241}Am lung source in Livermore plastic chest phantom and 10 min of measurement. On the right: reconstructed measurement geometry, written as MCNP$^{\mathrm{TM}}$ input file with *Anthropo*, and then visualized with Sabrina®

plate (serial number CZ215590). The slices displayed correspond to the middle of the lungs along the vertical axis. The central axis of the detector was placed within the slices displayed. The principal distances $L_{\max}$ and L_{med} are measured from the slices displayed, and $L_{\min}$ was obtained through averaging distance from the closest point of the lungs to the detector within the slice displayed and four points on the lung surface surrounding the closest point at the radius of 1 cm.

For these phantoms, the relative difference (data for phantom minus data for the patient) for counting efficiency (normalized by simulation data for the patient) for full absorption peaks of ^{241}Am (13.90, 17.54, 21.01, 26.30 and 59.54 keV) and ^{235}U (15.50, 89.90,93.30, 105.00, 109.16, 143.76, 163.33, 185.72 and 205.31 keV), are shown in Fig. 5. The error bars correspond to the statistical uncertainty (one standard deviation) of Monte Carlo calculations. The difference between the phantoms are caused by the differences of phantom anatomy, which proves the importance of uncertainties in lung counting even for relatively high energies and confirms the requirements of individually specified computational phantoms for lung counter calibration.

Considering the phantoms mentioned in this paper, the worst patient anatomy representation is provided by the Winfrith phantom, which has extremely small lungs, shifted to anterior direction along antero-posterior axis. Rather thick chest wall, related to $L_{\min}$ parameter (see Table II, Fig. 3), causes intensive absorption in low-energy range, where ratio of counting efficiency for the phantom and the patient is quickly decreasing when energy decreases (see Fig. 5). However, lungs in the Winfrith phantom are abnormally shifted to the front part of chest, which makes not only maximal distance $L_{\max}$, but also median distance,

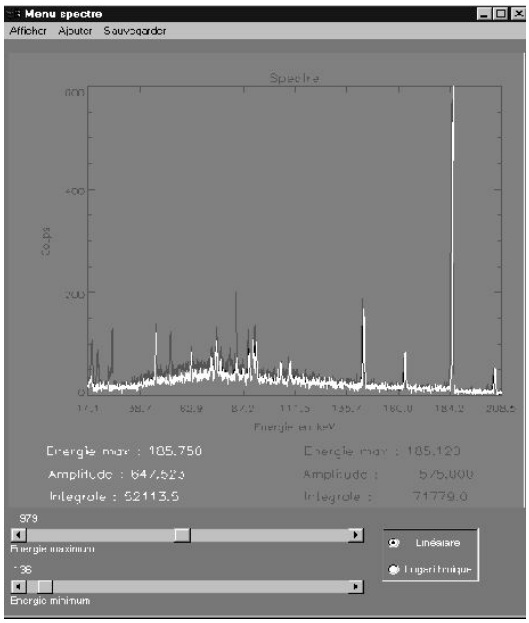

Figure 2. Comparison of calculation + background (white line) and experimental (dark line) spectra from uranium lung contamination (80 Bq of 93% enriched ^{235}U, 16 hours of measurement). Background, measured independently without source, is added to calculation spectrum

$L_{\mathrm{med}} = (L_{\mathrm{min}} + L_{\mathrm{max}})/2$, (see Fig. 3, Table II) shorter for the Winfrith phantom than for the patient. As a result, it provides a "compensation" of absorption for higher energies, which explains the apparent closeness of the patient and the Winfrith phantom in the 100–200 keV range.

The RANDO phantom lungs are also smaller and more deeply located in comparison to the patient (about 1 cm of shift for the three L parameters). As a result, in all the energy range counting efficiency is lower for the RANDO phantom than for the patient over the entire energy range.

The lungs of the Livermore phantom are more extended along anterior-posterior direction than for the patient (see Fig. 4). One the contrary, the lungs of the JAERI phantom are less extended along this direction in comparison to the patient. This provides higher efficiency for energies lower than 30 keV for the Livermore phantom than for the JAERI phantom, caused by longer L_{min} of the latter. In this energy range one can observe that efficiency for the Livermore phantom is almost equal to that for the patient. Contrary, longer L_{max} and L_{med} for the Livermore phantom than for the JAERI phantom provides additional absorption for the former in energy range 50–200 keV. As a result, counting efficiencies the Livermore and JAERI phantoms for such energies are almost equal, but they are 30% lower than for the patient.

3.3. Application of *Anthropo* for heterogeneous contamination study

In previous subsections the distribution of activity in lungs was considered to be uniform. However, in the case of real contamination by inhalation this distribution is likely to be heterogeneous. For example, aerosols are mostly deposited in lung alveoli (see ICRP Report 66 [12]), however, distribution of alveoli is

Table II. Characteristics of scanned phantoms

	Livermore Plate No. 3	JAERI with plate	RANDO	Winfrith	Patient
Whole body height, cm	177	168	175	175	Non available
Whole body weight, kg	76	63.5	73.5	72.5	74.5
Thickness of front soft tissue layer, $L_{\min}$, cm	3.6	3.7	4.3	3.8	3.0
Depth of back lung boundary, $L_{\max}$, cm	23.9	17.1	19.5	13.8	19.2
Median distance to the lungs, L_{med}, cm	13.7	10.4	11.9	8.9	11.1
Right lung volume, cm^3	2294	2002	1855	768	1849
Left lung volume, cm^3	1781	1689	1581	815	1292

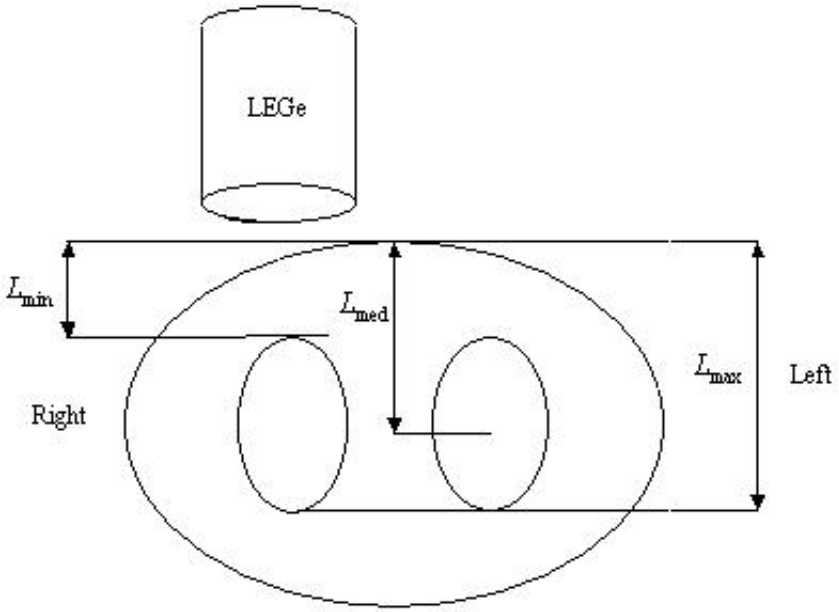

Figure 3. Scheme of principal distances from lungs to the front surface of thorax during whole body counting with low-energy germanium detector (LEGe). $L_{\min}$ is the minimal distance between source (lung) and front surface, it mostly determines counting efficiency for low energies. For higher energies, maximal distance $L_{\max}$ and median L_{med} are also essential

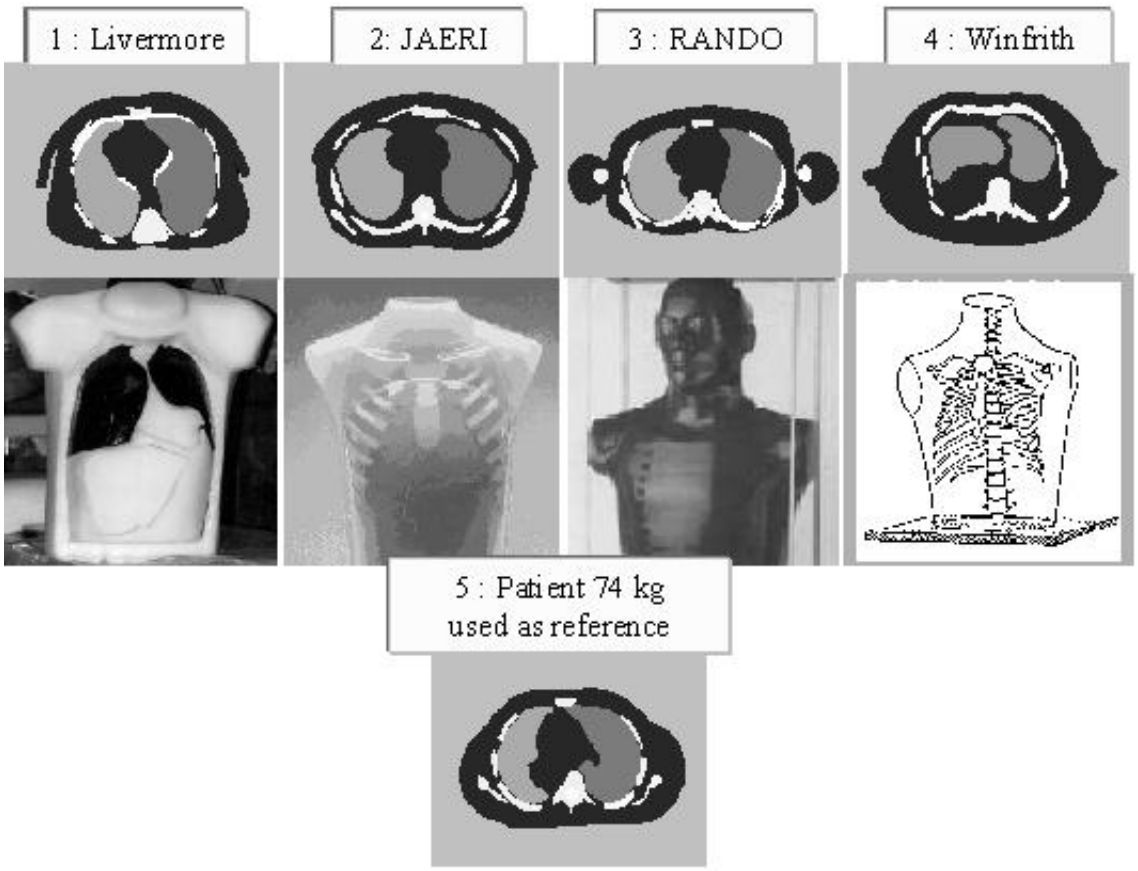

Figure 4. Images of phantoms scanned with CT device and segmented with DOSIGRAY®, loaded into *Anthropo* for MCNP^{TM} input file creation: Livermore plastic chest phantom (1), Jaeri plastic phantom (2), Rando whole body phantom (3), Winfrith hollow phantom, filled with tissue-equivalent powder (4), image of a real male patient weighing 74 kg (5)

not uniform through lungs.

To initiate the study of influence for contamination heterogeneities for lung counting results, several numerical experiments with two model types of contamination — surface and point — were done.

Calculations with surface source in lungs

For surface contamination, marginal part of lungs, located in lungs close to their boundaries, was separated from other parts of lungs by specifying lung margins of 1 and 2 cm width with DOSIGRAY®, which was followed by *Anthropo* segmentation (see Fig. 6). During calculations, the activity was considered to be

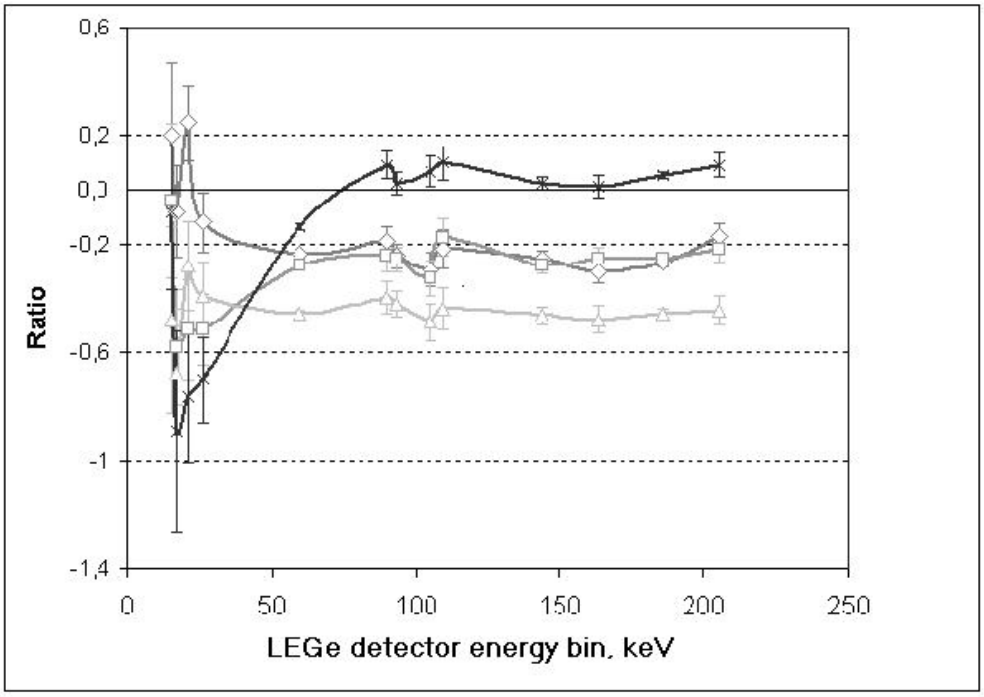

Figure 5. Calculated relative (normalized by simulation data for the patient) difference (data for phantom minus data for the patient) for counting efficiency for full absorption peaks of ^{235}U and ^{241}Am for different phantoms, processed with *Anthropo*: × — Winfrith, ◇ — Livermore, □ — JAERI, △ — RANDO

uniformly distributed through only the lung margins.

Figure 6. *Anthropo* representation of the Livermore phantom with plate #3, from left to right: no margins, 1 cm width lung margins, 2 cm width lung margins

The comparison of relative full absorption peak efficiencies, normalized by the same activity uniformly distributed through all the lungs, for different gamma rays emitted by ^{241}Am and ^{235}U, listed in the

previous section, LEGe spectrometer, placed in front of the right lung, is shown in Fig. 7. For energies lower than 20 keV due to the larger number of gamma rays emitted from the minimal distance to the detector $L_{\min}$, efficiency for surface contamination is higher than for uniform. As far as one can see, for energies higher than 20 keV almost no statistically significant difference has been found between surface and uniform contamination. The reason for it is that the importance of activity placed at median distance L_{med} increases for higher energies; and more activity at median distances is deposited for uniform contamination.

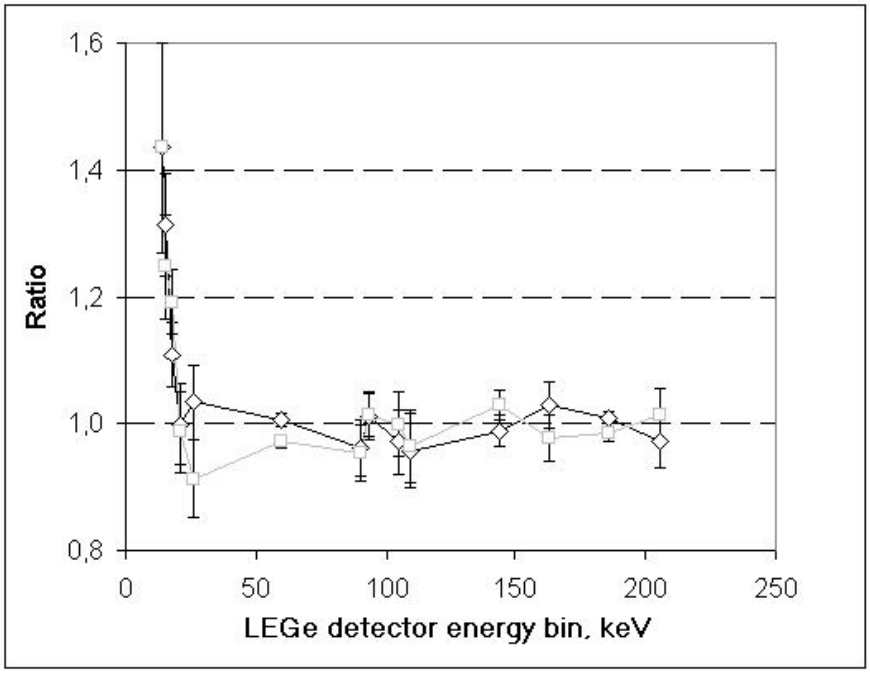

Figure 7. Calculated relative (normalized to 1.0 by simulation data for uniform lung contamination) counting efficiency for full absorption peaks of ^{235}U and ^{241}Am for surface lung contamination: □ — 1 cm width margin, ♢ — 2 cm width margin

Calculations with point source in lungs

Another studied geometry — multi-point source — represents the most extreme localisation of contamination, which might take place during inhalation with actinide-containing insoluble compound aerosol particles.

Calculations were done with 5 pairs of point sources placed in different parts of the lungs, each pair being put symmetrically — one source in right lung, the other in left (see Fig. 8, each point of the pair contains equal activity).

The comparison of relative full absorption peak efficiencies, normalized by the same activity, uniformly distributed in lung, for different point sources, containing ^{241}Am and ^{235}U, listed in the previous section, and LEGe spectrometer, placed in front of the right lung, is shown in Fig. 9 (logarithmic scale). The figure shows also the averaged response from point sources 1–5 (for hypothesis of activity equally distributed in 5

Figure 8. Point source positions in different slices in the Livermore phantom with plate #3 for calculations with point sources

pairs of point sources). As for previous geometries (Fig. 5 and 7), for energies lower than approximately 20 keV, the most critical parameter is source intensity at distances near $L_{\min}$. That is why for position 3, where the distance from the point source is approximately equal to $L_{\min}$, the efficiency quickly decreases with the energy (when $E < 20$ keV), but for other positions, where the distance form point source is longer than $L_{\min}$, the efficiency increases with the energy (when $E < 20$ keV).

For energies higher than 20 keV, the importance of source intensity on distances equal to L_{med} increases, so the dependence of efficiency is almost flat for every source position, except the closest position 3. For position 4 the efficiency is approximately equal to the efficiency for homogenous contamination.

As to the averaged response, for energies lower than 20 keV, the closest to the detector point source 3, playing the most important role in the contribution of response, causes the increase of response with decrease of energy. For energies higher than 20 keV point source 3 still contributes the major part of average response, causing slightly higher counting efficiency than for uniform source.

4. CONCLUSION AND OUTLOOK

Calibration associating voxel numerical phantoms with Monte Carlo calculations has already been suggested as a tool of solving *in vivo* measurement system x-ray and gamma-ray spectrometry calibration problems. It has been demonstrated that this approach has considerable potential for calibration of *in vivo* counting systems for measuring low energy x-ray and gamma-ray emitters in the lung. The work described in this paper was carried out with a view to extend the use of this principle to construction of numerical phantoms based on real anatomical data relating to the individuals to be measured, using scanned images. The interface designed makes it possible to automatically create a MCNP4c$^{\mathrm{TM}}$ input file with complex three-dimensional phantom geometry reconstituted from the scanned images.

The results of first simulations are encouraging. For low and medium energies simulated spectra have been obtained in modeling of lung count measurements on phantoms contaminated with ^{241}Am and ^{235}U. The calculation results are comparable to those obtained by experimentation. The relative error between simulation and experimentation is less than 15%.

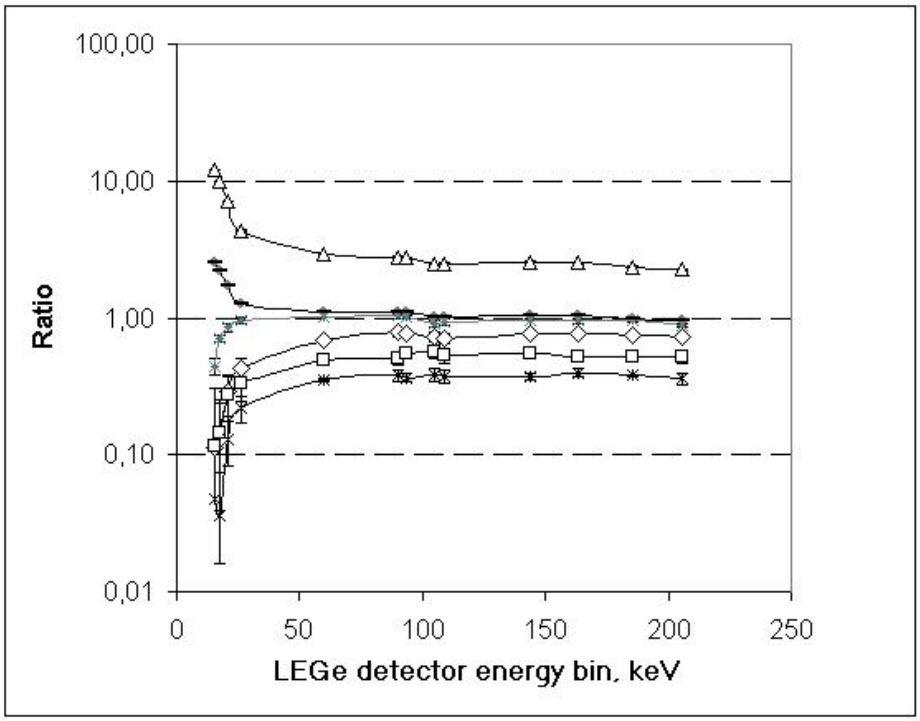

Figure 9. Calculated relative (normalized to 1.0 by simulation data for uniform lung contamination) counting efficiency for full absorption peaks of ^{235}U and ^{241}Am for point contamination in lungs: $\diamondsuit$ — position 1, $\square$ — position 2, $\triangle$ — position 3, $\times$ — position 4, $*$ — position 5, $-$ — averaged response from point sources 1–5

The study of uncertainties influencing lung counting results were shown through the comparison of calculated efficiency for both low and high energies with different phantoms, scanned and processed with *Anthropo*, as well as with different source configurations. The difference between calculation results in different geometries proves the importance of uncertainties in lung counting even for relatively high energies and confirms the requirements of individually specified computational phantoms for lung counter calibration.

Consequently, as a result of its flexibility in accepting complex geometries, the method developed not only represents a diagnostic tool for *in vivo* measurement, but also opens up new possibilities such as optimisation of detection systems, study of contamination with mixed actinides and any other simulation using MCNP4c$^{\mathrm{TM}}$ where complex geometry is derived from a set of CT and/or MRI images.

ACKNOWLEDGEMENTS

The authors would like to appreciate the friendly assistance of G. L. Genicot from Belgian Nuclear Research Center (SCK·CEN), Mol, Belgium, who provided for scanning the torso phantom developed at Winfrith Technology Center, UK. Other thanks must be given to Medical Imaging Service of *Hôpital d'Instruction des Armées Percy*, Clamart, France, and its head, D. Jeanbourquin, who provided CT scan of

the phantoms. The authors are also very grateful to the team of Gustave Roussy Cancer Research Institute in Villejuif, who provided DOSIGRAY® software for IRSN.

REFERENCES

[1] D. Franck, L. de Carlan, Ph. Berard, C. Dousse, P. Pihet, N. Razafindralambo et R. Soulié, "Les mesures anthroporadiométriques dans les basses énergies : évolution technologique et bases des recherches futures,"*Radioprotection*, **32**, pp. 685-696 (1997).

[2] C. Kang, D. Newton, A. J. Warner, T. A. Absolom, D. A. Druchten, A. L. Anderson, and E. E. Palmer, "A comparison of techniques in the assessment of chest wall thickness and composition," *Health Phys*, **64**, pp. 406-411 (1993).

[3] L. R. Vikers, "The gender-specific chest wall thickness prediction equations for routine measurements of ^{239}Pu and ^{241}Am within the lung using HPGe detectors," *Health Phys*, **70**, p. 685-427 (1996).

[4] M. W. Mallett, D. P. Hickman, D. A Kruchten and J. W. Poston, "Development of a method for calibrating *in vivo* measurement systems using magnetic resonance imaging and Monte Carlo calculations," *Health Phys*, **68**, pp. 773-785 (1995).

[5] J. C. Hunt, I. Malatova, and S. Foltanova, "Calculation and measurement of calibration factors for bone surface seeking low energy gamma emitters and determination of ^{241}Am activity in a real case of internal contamination," *Radiat Prot Dosim*, **82**, pp. 215-218 (1999).

[6] N. Borisov, D. Franck, L. de Carlan and L. Laval, "A new Graphical User Interface for fast construction of computation phantoms and MCNP calculations: application to calibration of *in vivo* measurement systems," *Health Phys*, **83**, pp. 272-280 (2002).

[7] PV-Wave®, Version 7.0. Visual Numerics® inc. *User's Guide*. Houston, TX, (1999).

[8] J. F. Briesmeister, *MCNP — A general Monte Carlo N-particle transport code, version 4c*, LANL Memorandum. Los Alamos National Laboratory, LA-13709-M (2000).

[9] International Commission on Radiation Units and Measurements, *Tissue substitutes in radiation dosimetry and measurements (ICRU Report 44)*, ICRU Publication, Bethesda (1989).

[10] A. V. Kenneth, *User's guide for Sabrina®. Version 3.56*, Radiation Transport Group -Applied Theoretical Physics Division - Los Alamos National Laboratory, LA-UR-93-3696 (1994).

[11] International Commission on Radiation Units and Measurements. *Phantoms and computational models in therapy, diagnosis and protection (ICRU Report 48)*, ICRU Publication, Bethesda (1992).

[12] International Commission on Radiation Protection. *Human respiratory tract model for radiological protection (ICRP Publication 66), Annals of the ICRP*, **24**, No 1-4 (1994).